Actinic extreme ultraviolet mask inspection beyond 0.25 numerical aperture

K. A. Goldberg,[a] P. Naulleau, I. Mochi, E. H. Anderson, S. B. Rekawa, C. D. Kemp, and R. F. Gunion
Mail Stop 2-400, Lawrence Berkeley National Laboratory, Berkeley, California 94720

H.-S. Han
Photomask Team, Samsung Electronics, Ban-Wol, Hwasung, Kyunggi 445-701, Republic of Korea

S. Huh
SEMATECH, 255 Fuller Road, Suite 309, Albany, New York 12203

(Received 17 June 2008; accepted 22 September 2008; published 1 December 2008)

The SEMATECH Berkeley actinic inspection tool (AIT) is an extreme ultraviolet (EUV)-wavelength mask inspection microscope designed for direct aerial image measurements and precommercial EUV mask research. Operating on a synchrotron bending magnet beamline, the AIT uses an off-axis Fresnel zoneplate lens to project a high-magnification EUV image directly onto a charge coupled device camera. The authors present the results of recent system upgrades that have improved the imaging resolution, illumination uniformity, and partial coherence. Benchmarking tests show image contrast above 75% for 100 nm mask features and significant improvements and across the full range of measured sizes. The zoneplate lens has been replaced by an array of user-selectable zoneplates with higher magnification and numerical aperture (NA) values up to 0.0875, emulating the spatial resolution of a 0.35 NA 4× EUV stepper. Illumination uniformity is above 90% for mask areas 2 μm wide and smaller. An angle-scanning mirror reduces the high coherence of the synchrotron beamline light source giving measured σ values of approximately 0.125 at 0.0875 NA. © *2008 American Vacuum Society.* [DOI: 10.1116/1.3002490]

I. INTRODUCTION

Mask research is central to the development and commercialization of extreme ultraviolet (EUV) lithography. The resonant-reflective nature of EUV multilayer coatings and the wavelength-specific properties of materials used to create EUV masks make it necessary to conduct research at the operational EUV wavelength. Therefore, the development and optimization of EUV mask architectures and defect detection and mitigation technologies currently rely on precommercial printing and at-wavelength inspection tools such as the SEMATECH Berkeley microfield exposure tool (MET)[1] and the SEMATECH Berkeley actinic inspection tool (AIT).[2–4]

The AIT is a dual-mode microscope that can operate in scanning-beam and imaging modes. In the scanning-beam mode,[4] the EUV beam is focused onto a single point on the mask with a beam diameter of 1–5 μm. The reflected signal, including both *bright-field* specular reflection and *dark-field* scattered light, is recorded by a three-element photodiode as the mask translates below the focused beam. In imaging mode[3] the AIT operates as an EUV Fresnel zoneplate (holographic lens) microscope: the submillimeter diffractive lens sits above the mask surface and projects an image of the illuminated mask with high magnification, onto an EUV-sensitive charge coupled device (CCD) camera.

The AIT is now routinely used in studies of pattern defect repair,[5] sensitivity to buried, substrate phase defects,[6,7] mask contrast, and aerial image properties.

[a]Electronic mail: kagoldberg@lbl.gov.

A. System description

Detailed descriptions of the AIT optical system and performance specifications in imaging mode have been presented previously.[2–4] The AIT uses a synchrotron bending magnet beamline at the Advanced Light Source, at Lawrence Berkeley National Laboratory (LBNL). A monochromator provides an EUV illumination with a tunable wavelength and bandwidth: the AIT typically operates at 13.4 nm wavelength with a bandwidth, $\lambda/\Delta\lambda$, of 1600. The narrow bandwidth is required to avoid chromatic aberration from the zoneplate lens.

Glancing incidence beamline mirrors, including a Kirkpatrick–Baez (KB) mirror pair create an intermediate focus of approximately 100×300 μm, which is reimaged onto the mask by a 20× demagnification, EUV Schwarzschild objective. Using an off-axis subaperture of the Schwarzschild objective, the central ray of the illuminating beam is inclined at 6° from vertical as it reaches the upward-facing mask. In imaging mode, we typically operate with the mask surface 200–400 μm below the Schwarzschild's focal plane to provide a larger and more uniform illumination area.

In the AIT, an off-axis zoneplate lens with a focal length of 1 mm or less projects a highly magnified image of the mask surface onto an EUV CCD camera. The illuminating beam passes downward through an unpatterned region of the zoneplate membrane. The zoneplate is positioned to collect the reflected light and focus it to a plane several hundred millimeters away. The zoneplate's off-axis design provides angular separation of the various diffraction orders so that the focusing first order light does not overlap the other orders

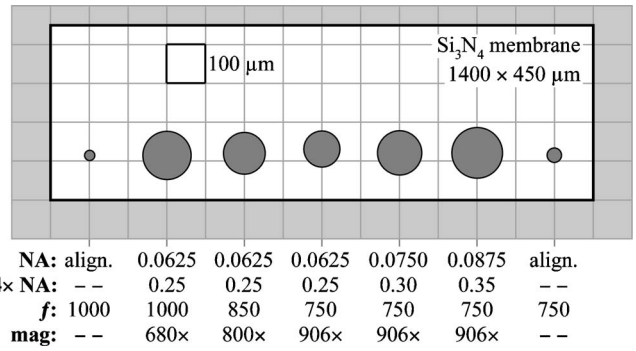

FIG. 1. A new zoneplate array design allows one of five different zoneplates to be selected. Zoneplates are held within 1 mm above the mask. The illuminating beam passes downward through the unpatterned portion of the Si_3N_4 membrane. Reflected light is collected by one of the off-axis zoneplates and focused on the CCD. Two small zoneplates on the ends serve as distinct alignment features.

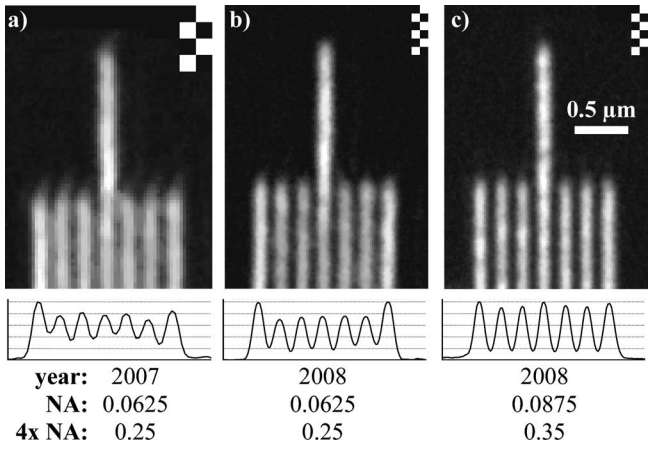

FIG. 2. Image details from 100 nm linewidth elbow patterns recorded (a) before and [(b) and (c)] after the AIT upgrades. Smaller CCD pixels and higher magnification zoneplate lenses result in higher pixel density. Each square in the checker patterns is five CCD pixels wide in the raw data. Regions near the bottom of the images were averaged vertically to produce the profiles.

in the image plane. A small, 45°, multilayer-coated turning mirror is positioned between the Schwarzschild housing and the mask, and reflects the light horizontally toward the CCD.

The AIT routinely records 250–350 high-quality images in numerous through-focus series per 8 h shift. Typical exposure times range from 0.5 s during alignment to approximately 25 s for high-resolution images.

B. 2008 upgrades

Upgrades conducted in 2008 have made significant improvements in the imaging performance, including resolution and contrast, and illumination uniformity and partial coherence. The most significant additions were a new zoneplate design, a CCD camera with higher pixel density, and an actuator to continuously scan the angle of the horizontal KB mirror. Measurements performed to quantify these improvements are the primary subject of this paper.

In a new zoneplate design (Fig. 1), a single silicon-nitride membrane window in an etched Si wafer was patterned with an array of five zoneplates, each with different optical properties. The zoneplate array allows the operator to select from three different numerical aperture (NA) values at highest magnification. Lenses with NA values of 0.0625, 0.075, and 0.0875 emulate the spatial resolution of a 4× EUV stepper with 0.25, 0.30, and 0.35 NA, respectively.

One goal of the new design is to achieve higher pixel density in the recorded images. A new EUV CCD camera was installed with 13.5 μm pixel width, replacing the 20 μm pixel camera used before 2008. The new zoneplates are designed with a 33% higher magnification ratio. Combining the higher imaging magnification with smaller pixels, the equivalent mask plane pixel density is now 16 nm/pixel, compared with 31 nm/pixel in 2007. The diffraction-limited resolution of the AIT zoneplates is always several times larger than this pixel equivalent size, so the image is adequately sampled. For example, at 0.35 NA, 4× equivalent, the true NA of the zoneplate is 0.0875, the *Rayleigh resolution* ($0.61\lambda/\mathrm{NA}$) is 94 nm, and the outer zone width Δr of this 6° off-axis lens is 35 nm.

Figure 2 shows three image details of similar dark-field mask features with 100 nm line width, recorded before and after the upgrade, and with the higher-NA zoneplate lens.

To improve the illumination uniformity and to reduce the high degree of coherence, the stage that holds the horizontal element of the KB mirror pair was retrofitted with a small, in-vacuum scanning motor that controls the tilt angle. We oscillate the tilt angle during exposures, scanning through a range of illumination angles.

C. Carbon contamination

Although power levels in the AIT are relatively low, compared to the proposed commercial EUV lithography tools—not more than tens of nanowatts reach the mask—intensive use over a period of months to years leads to the buildup of carbon contamination. Contamination causes reduced flux levels and nonuniform illumination, discussed in the following section. We take several steps to mitigate carbon contamination: ultrahigh vacuum protocols are followed to limit contamination and to avoid outgassing materials; only narrow-band EUV illumination is used to avoid out of band radiation; and a low partial pressure of oxygen gas, less than 10^{-4} Torr, flows into the endstation in the vicinity of the 45° mirror that precedes the Schwarzschild objective.

Despite these measures, we observe the buildup of carbon contamination, and we periodically replace the accessible optical elements in the endstation. Recently, after approximately 240 h of use, carbon was visible on the zoneplate membrane. The abovementioned 45° turning mirror, however, showed no visible carbon buildup during the same period. Furthermore, we believe that the reflectivity and uniformity of the Schwarzschild objective's pupil have been degraded over time as evidenced by the incident-angle dependence of the mask illumination intensity and the nonuniformities in the static illumination pattern. That element, however, cannot easily be replaced or cleaned *in situ*.

II. ILLUMINATION UNIFORMITY

Illumination uniformity is a property that affects all measurements made from the recorded aerial images. Achieving uniform illumination in the AIT is challenging because of the nature of the existing synchrotron-beamline illumination system. The light undergoes nine reflections between the bending magnet source and the mask. The beam is also transmitted through the pattern-free region of a silicon-nitride membrane that contains the zoneplate lenses. Different types of surface contamination, imperfect focusing, and other sources of nonuniformity are difficult to avoid or eliminate completely.

To improve uniformity, we have installed an angle-scanning motor onto the stage that supports the horizontal KB mirror. During the high-resolution exposures, small angle changes sweep the illumination pattern in the *x*-direction. The scan rate depends on the amplitude: 1.7 Hz is a typical frequency, and in a 25 s exposure, the angle scanner completes almost 15 cycles.

A. Illumination uniformity measurement

Using images recorded from a blank EUV mask, we can quantify the measured illumination uniformity as a function of the area of interest, with and without the actuation of the angle-scanning mirror. To perform this measurement, two images close to best focus were selected from through-focus series, and uniformity analysis was performed on subdomains of the full images. Both images were 25 s exposures, recorded a few minutes apart. One of the images was recorded with the angle-scanning mirror active and the other, with the mirror in a static, centered position.

Square subdomains were extracted from near the centers of the images with widths corresponding to the following mask dimensions: 1, 2, 3, 5, 8, and 10 μm. (The full width of the 2048×2048 pixel images corresponds to approximately 32.8 μm, and the linear scale is approximately 16 nm/pixel.) For each image and subdomain size being evaluated, 100 similar subdomains were extracted and examined: the centers of these overlapping subdomains were spaced in a 10×10 grid with 20 pixel steps.

For this analysis, *uniformity* is defined as the ratio of the minimum value to the maximum value within each subdomain. Figure 3 contains the average measured uniformity for the six region sizes calculated from each image. The standard deviation values for the data points are indicated by the error bar lengths. As expected, smaller regions achieve higher average uniformity. Values above 90% were measured for region widths of 2 μm and below. In the static illumination cases, the large standard deviations of the 2, 3, and 5 μm subdomains reveal the much greater variability in the neighboring regions that the scanning illumination addresses. The data show that illumination angle scanning effectively smoothes the nonuniformities that occur in the 2–5 μm length scale.

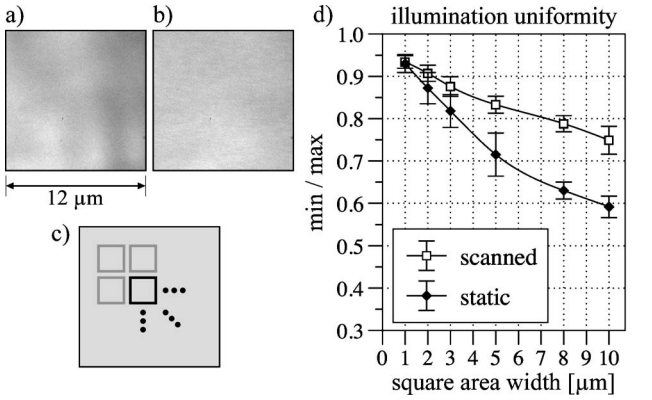

FIG. 3. Illumination uniformity calculated from image subregions of a blank mask. Details corresponding to 12-μm-wide mask regions with (a) static and (b) scanning illumination. As shown schematically (c), the minimum and maximum intensity values found within 100 different adjacent or overlapping regions near the center of the CCD are used to compute the average and standard deviation (d) for a range of mask-region widths.

III. CONTRAST TRANSFER FUNCTION

The contrast transfer function (CTF) of an optical system is the ratio of the contrast in the image to that in the object as a function of the feature size. The more familiar *modulation transfer function* (MTF) is strictly defined for incoherent illumination conditions ($\sigma=\infty$). The CTF of a high-quality imaging system is a function of its illumination coherence properties, the pupil's shape and numerical aperture, and the incident light wavelength. Coherent or nearly coherently illuminated aberration-free systems maintain high contrast with a sharp drop near the resolution limit. Aberrations reduce the contrast in a manner that varies with both the direction and size of features being imaged.

A. CTF measurement

Hundreds of images were recorded to assess the AIT's CTF using mask linewidths from 100 to 500 nm and two different elbow pattern orientations. Contrast measurement involves (1) the extraction of elbow pattern regions from each image, (2) intensity normalization across the line region, and (3) the evaluation of the contrast for the central three elbow lines, averaged over several pixels along the length of the line. From the four available pattern directions, the analysis selected the peak contrast at best focus for each measurement series. Note that the object (mask) modulation is slightly less than 100% (97.4%), based on the measured light intensity in the pure absorber regions.[3]

B. Dark-field CTF before and after upgrades

Dark-field measurements are shown in Fig. 4. A direct comparison of contrast data recorded before and after the upgrades, using similar 0.0625 NA zoneplate lenses, shows that a significant increase in contrast has been achieved. Data from the new 0.0875 NA zoneplate are also shown in Fig. 5. Although the higher-NA lens achieves greater contrast for the smallest measured features (above 75% contrast for 100 nm CD), the lower NA lens has slightly higher contrast

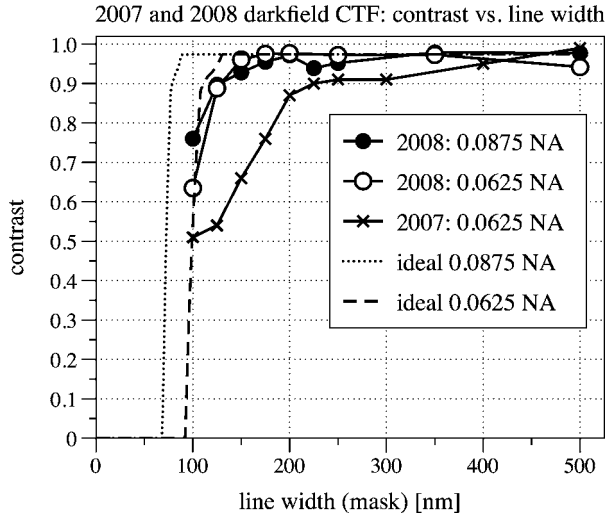

FIG. 4. Dark-field CTF computed from elbow patterns with mask linewidths between 100 and 500 nm. In each case the highest measured contrast from four available elbow directions is shown. The dashed curves show the theoretical performance calculated with $\sigma_y=0$, and $\sigma_x=0.125$ and 0.175 for the 0.0625 NA and 0.0875 NA cases, respectively.

for larger features. An increased aberration magnitude associated with the higher-NA lens may be responsible for the lower contrast. For comparison, the dashed curves in the figure show the calculated ideal CTF performance of two systems: (a) 0.0625 NA and $(\sigma_x,\sigma_y)=(0,0.175)$, and (b) 0.0875 NA and $(\sigma_x,\sigma_y)=(0,0.125)$.

C. Lower contrast in bright field

Compared with the dark-field measurements, the data show lower bright-field contrast (typically by several percent). The difference is consistent with the 2%–3% flare magnitude measured in a similar zoneplate lens used in 2007.[3] In addition, a secondary source of contrast reduction that affected the bright-field measurements was a weak but

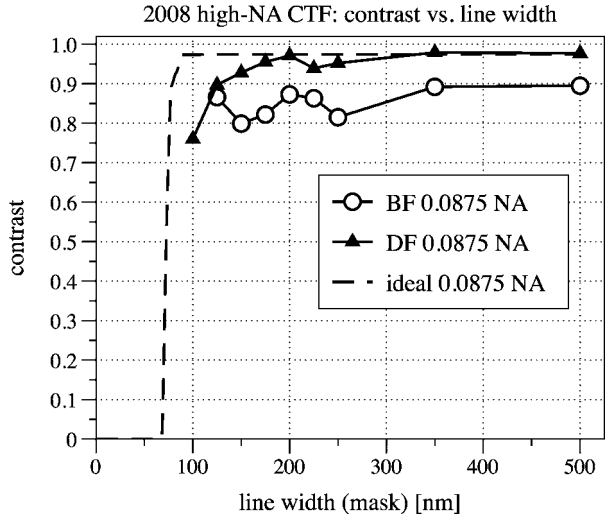

FIG. 5. Measured bright-field (BF) and dark-field (DF) CTF data from the 0.0875 NA zoneplate.

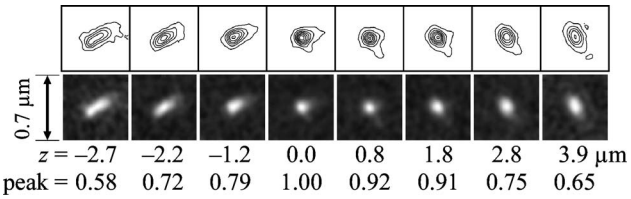

FIG. 6. Contours and image details from a through-focus series of a single, 175 nm square contact. Images are individually scaled. The contour levels are drawn in 0.125 steps, normalized to the peak intensity of the series. The relative focal displacement (z) and scaled peak magnitude values are given.

persistent reflected beam overlap that came from an unobstructed light path reaching the CCD camera. (A new zoneplate membrane design has been created to block this unwanted light.)

The limits of the test mask's quality were not addressed in this study. Dark-field elbows were clearly resolved as small as 100 nm CD. However, bright-field features below 125 nm were not resolved on the mask, and the 125 nm features were irregular.

D. Aberrations

Aberrations in the AIT imaging depend sensitively on the system alignment, including the illumination angles and the zoneplate position. Even if the zoneplate were aberration-free, displacements and misalignment can introduce aberrations. Furthermore, small variations in the aberrations across the field of view are an unavoidable consequence of using a single lens imaging system. We expect that aberrations caused by misalignment would grow as powers of the NA value and would therefore impact the high-NA imaging more severely.

When these data were collected, astigmatism was the dominant aberration near the center of the AIT's field of view. Depending on the elbow feature size, astigmatism causes several microns of astigmatic displacement (i.e., the peak contrast for orthogonal pattern directions occurs in focal planes separated by a few microns). Figure 6 shows through-focus images of a 175 nm square contact through focus in which the presence of astigmatism is clear, and a small comalike effect is also visible. The detailed quantification of these aberrations is now in progress.

IV. ILLUMINATION COHERENCE

The bending-magnet beamline source provides a high degree of illumination coherence. The coherence is reduced in the x-direction by the action of the angle-scanning mirror, described in Sec. II. Quantifying the illumination coherence properties is essential for imaging data analysis and for comparison with printing and modeling.

We assess the degree of partial coherence by studying the contrast of dense-line features in large, through-focus series.[3] The observed contrast oscillates between high and low values as the mask moves through focus. While coherent illumination ($\sigma\approx 0$) produces high contrast peaks over a large

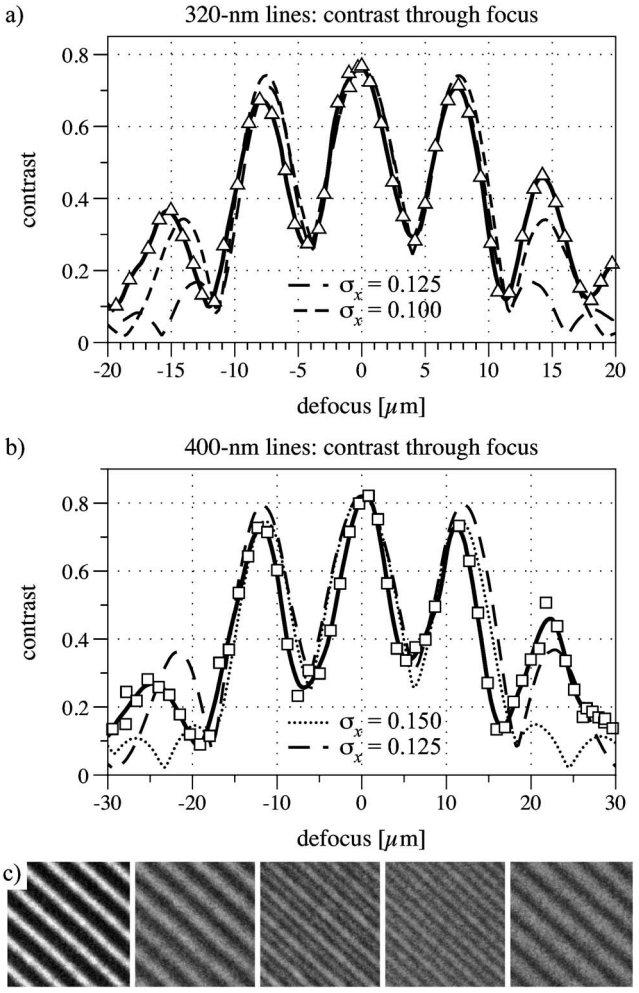

FIG. 7. The illumination partial coherence is determined by studying dense-line contrast through focus. Experimental data (open symbols) are compared with models (dashed lines) having different σ_x values. (a) 320 nm and (b) 400 nm lines provide consistent results showing that σ_x is close to 0.125 for the 0.0875 NA (0.35 NA 4× equivalent) lens. (c) 2 μm^2 image details from the through-focus series are shown. Contrast calculations are based on extracted image subdomains, like this.

focal range, partially coherent illumination produces a characteristic series of diminishing peaks that can reveal the σ value by comparison with modeling.

We recorded several such series using large, dense-line patterns with 240, 320, and 400 nm linewidths, moving as far as 30 μm out of focus in both directions. The 0.0875 NA zoneplate lens was used for these measurements. For comparison with the experimental data, calculations were performed using the same wavelength, distances, NA, and mask pattern, and a range of σ_x values chosen to capture the behavior of the angle-scanning horizontal KB mirror. Knowing that the illumination angles are static in the y-direction, we used the approximation that σ_y=0. Data from measurements and modeling are shown in Fig. 7. For 320 and 400 nm linewidths, the experimental data are compared with two model σ_x values, as indicated. In each case, a scaling factor has been applied to the model data to match the experimental contrast at best focus. (The model value would otherwise be unity at best focus.) Figure 7(c) contains five image details, approximately 2 μm wide, which have been extracted from near the center of several images in the through-focus series.

The modeling comparisons show that σ_x values close to 0.125 are a good approximation for the coherence properties we observed. Discrepancies between the measured data and the model likely come from aberrations in the zoneplate lens and its alignment and from imperfect z actuation over the large through-focus distance.

It is important to note that the partial coherence scales inversely with the imaging lens' NA. Since the measurements presented here were made using the 0.0875 NA lens, σ_x will be higher when a lower-NA zoneplate is used and all other conditions are the same. For example, with the 0.075 or 0.0625 NA lenses, σ_x should grow to 0.146 and 0.175, respectively.

V. CONCLUSION

Recent upgrades to the SEMATECH Berkeley AIT have improved its performance in the areas of aerial image resolution, illumination uniformity, and partial coherence. Using a variety of new, high-NA zoneplate lenses, the AIT emulates the resolution of EUV lithography tools with NA values up to 0.35. The AIT provides above 90% uniformity for a 2 μm square (mask) area and above 87% for a 3 μm area. Dense-line contrast measurements through focus were compared with modeling to show that the x-direction partial coherence σ_x is approximately 0.125 for the 0.35 NA 4× equivalent (0.0875 NA) lens. Based on that measurement, we predict that σ_x is 0.175 for the 0.25 NA 4× equivalent (0.0625 NA) lens.

ACKNOWLEDGMENTS

The authors gratefully acknowledge the support of SEMATECH, including Stefan Wurm, Kim Dean, and others who worked to ensure the ongoing success of this project. LBNL team members who have been instrumental in the development of the AIT include Paul Denham, Rene Delano, Brian Hoef, and Kevin Bradley. The authors would also like to thank Bruno LaFontaine of AMD, Ted Liang of Intel, and Pat Kearney of SEMATECH for providing the masks used in this research. This work was funded by SEMATECH under Project No. LITH-343S2 and was performed under the auspices of the U.S. Department of Energy by University of California Lawrence Berkeley National Laboratory.

[1]P. P. Naulleau *et al.*,Proc. SPIE **6921**, 69213N (2008).
[2]K. A. Goldberg, A. Barty, Y. Liu, P. Kearney, Y. Tezuka, T. Terasawa, J. S. Taylor, H.-S. Han, and O. R. WoodII, J. Vac. Sci. Technol. B **24**, 2824 (2006).
[3]K. A. Goldberg *et al.*, Proc. SPIE **6730**, 67305E (2007).
[4]K. A. Goldberg, S. B. Rekawa, C. D. Kemp, A. Barty, E. H. Anderson, P. Kearney, and H.-S. Han, Proc. SPIE **6921**, 69213U (2008).
[5]G.-S. Yoon *et al.*, *EUVL Symposium 2007*, Sapporo, Japan 31 October 2007 (unpublished).
[6]W. Cho, H.-S. Han, K. A. Goldberg, P. A. Kearney, and C.-U. Jeon, Proc. SPIE **6730**, 673013 (2007).
[7]H.-S. Han, W. Cho, K. A. Goldberg, E. M. Gullikson, C.-U. Jeon, and S. Wurm, Proc. SPIE **6921**, 62911Y (2008).